

The Glauber model and heavy ion reaction and elastic scattering cross sections

Ajay Mehndiratta^a, Prashant Shukla^{b,c,*}

^a*Physics Department, Indian Institute of Technology, Guwahati, India*

^b*Nuclear Physics Division, Bhabha Atomic Research Centre, Mumbai 400085, India.*

^c*Homi Bhabha National Institute, Anushakti Nagar, Mumbai 400094, India.*

Abstract

We revisit the Glauber model to study the heavy ion reaction cross sections and elastic scattering angular distributions at low and intermediate energies. The Glauber model takes nucleon-nucleon cross sections and nuclear densities as inputs and has no free parameter and thus can predict the cross sections for unknown systems. The Glauber model works at low energies down to Coulomb barrier with very simple modifications. We present new parametrization of measured total cross sections as well as ratio of real to imaginary parts of the scattering amplitudes for pp and np collisions as a function of nucleon kinetic energy. The nuclear (charge) densities obtained by electron scattering form factors measured in large momentum transfer range are used in the calculations. The heavy ion reaction cross sections are calculated for light and heavy systems and are compared with available data measured over large energy range. The model gives excellent description of the data. The elastic scattering angular distributions are calculated for various systems at different energies. The model gives good description of the data at small momentum transfer but the calculations deviate from the data at large momentum transfer.

Keywords: Glauber model, heavy ion reaction cross section, elastic scattering

*Corresponding author

Email address: pshukla@barc.gov.in (Prashant Shukla)

1. Introduction

The Glauber model [1] is a semi classical model picturing the nuclei moving in a straight line trajectory along the collision direction and describes nucleus-nucleus interaction [2] in terms of nucleon-nucleon (NN) interactions. At high energies it is used to obtain total nucleus-nucleus cross section and geometric properties of the collisions such as the number of participants and binary NN collisions as a function of impact parameter [see e.g. [3, 4, 5]]. At low energies, the straight line trajectory is assumed at the Coulomb distance of closest approach between the two nuclei [6, 7]. The non eikonal nature of the trajectory is taken into account using a simple prescription given in Ref. [8]. This Coulomb Modified Glauber Model (CMGM) has been widely used in the literature [9, 10, 11, 12]. The work in Ref. [13] presents a systematic calculation of reaction cross section using CMGM. The Glauber model has no free parameter and thus has a variety of applications. It is used to extract the radii of unstable nuclei from measured total or reaction cross sections [14, 15, 16]. The Glauber model formalism together with the measured cross section is frequently used as a tool to test various forms of relativistic mean field densities [17, 18, 19]. It is also a useful tool to study the shape deformation of nuclei [20, 21]. The Glauber approach is similar to microscopic optical model approach which is used to study various nuclear reaction mechanisms [22]. The elastic scattering data are mostly interpreted in terms of optical model potential where the real part is commonly taken as double folding potential. Such formalism uses an imaginary potential with three free parameters and reproduces the diffractive patterns up to large angles as shown in the work of Ref. [23] for the elastic scattering of $^{16}\text{O} + ^{16}\text{O}$ at incident energies ranging from 124 to 1120 MeV. There are numerous attempts to explain the elastic scattering angular distributions of light nuclei using the Glauber model [24]. To have a better agreement with the data, the NN scattering amplitude is modified to include phase variation [25]. The isospin effects in NN scattering process have small impact on the cross sections as shown in the work of Ref. [26] which calculates the reaction cross section at intermediate

energy to study the medium effects on NN scattering cross sections. Ref. [27] describes the elastic scattering angular distributions of $^{16}\text{O} + ^{16}\text{O}$ and $^{12}\text{C} + ^{12}\text{C}$ using an NN phase shift function having three free parameters. A detailed study in the Ref. [28] presents a Monte Carlo Glauber model calculations of angular distributions of elastic scattering of α on light and heavy nuclei. The Monte Carlo approach includes the geometric fluctuations but is expected to give similar results as optical Glauber model at low energies. On comparison with the data this work concludes that the angular distributions can be predicted only up to certain angles. To get a better agreement at higher angles one may require more parameters as in Ref. [27].

In view of the importance and wide applicability of the model, we extend reaction cross section study of work in Ref. [13] for many more systems and collisions energies. We also calculate elastic scattering angular distributions, a study similar to the work of Ref. [28] but for many more systems. The nucleon-nucleon cross sections σ_{nn} , σ_{pp} and σ_{np} are the most important inputs in the calculations. We present simple parametrizations for the total cross sections as well for the ratio of real to imaginary parts of the scattering amplitudes for pp and np collisions using a large set of measurements and make a comparison with those available in the literature [7, 29]. The nuclear (charge) densities obtained by electron scattering form factors measured in large momentum transfer range are used in the calculations [30, 31]. For few systems we use three parameter Fermi density (3pF) in contrast to two parameter Fermi (2pF) density and Gaussian densities used in previous studies. The center of mass correction which is important for light systems has also been taken into account [32]. The reaction cross section and the elastic scattering angular distributions are obtained at many energies and are compared with the data to test the reliability of the model and the input parameters for many cases of stable nuclei.

2. The Glauber Model

The Glauber model gives the probability for occurrence of a nucleon-nucleon collision when the nuclei A and B collide at an impact parameter \mathbf{b} relative to each other which is determined to be [3, 4]

$$T(b)\bar{\sigma}_{NN} = \int \rho_A^z(\mathbf{b}_A)d\mathbf{b}_A \rho_B^z(\mathbf{b}_B)d\mathbf{b}_B t(\mathbf{b} - \mathbf{b}_A + \mathbf{b}_B) \bar{\sigma}_{NN}. \quad (1)$$

Here, $\rho_A^z(\mathbf{b}_A)$ and $\rho_B^z(\mathbf{b}_B)$ are the z-integrated densities of projectile and target nuclei respectively. $t(\mathbf{b})d\mathbf{b}$ is the probability for having a nucleon-nucleon collision within the transverse area element $d\mathbf{b}$ when one nucleon approaches at an impact parameter \mathbf{b} relative to another nucleon. All these distribution functions are normalized to one. Here $\bar{\sigma}_{NN}$ is the average total nucleon nucleon cross section.

The total reaction cross section σ_R can be written as

$$\begin{aligned} \sigma_R &= 2\pi \int b db (1 - |S(b)|^2), \\ &= \frac{\pi}{k^2} \sum_{l=0}^{\infty} (2l+1)(1 - |S_l|^2). \end{aligned}$$

The scattering matrix S_l or $S(b)$ where $bk = (l + 1/2)$ is given by

$$S(b) = \exp(i\chi(b)). \quad (2)$$

The Glauber phase shift $\chi(b)$ can be written as

$$\chi(b) = \frac{1}{2} \bar{\sigma}_{NN} (\bar{\alpha}_{NN} + i) AB T(b). \quad (3)$$

Here, $\bar{\alpha}_{NN}$ is the ratio of real to imaginary part of NN scattering amplitude which does not appear in the calculations of reaction cross section but is important for elastic scattering angular distribution.

In momentum space, $T(b)$ is derived as [13]

$$T(b) = \frac{1}{2\pi} \int J_0(qb) S_A(\mathbf{q}) S_B(-\mathbf{q}) f_{NN}(q) q dq. \quad (4)$$

Here, $S_A(q)$ and $S_B(-q)$ are the Fourier transforms of the nuclear densities and $J_0(qb) = 1/2\pi \int \exp(-qb \cos \phi) d\phi$ is the cylindrical Bessel function of zeroth

order. The function $f_{NN}(q)$ is the Fourier transform of the profile function $t(\mathbf{b})$ and gives the q dependence of NN scattering amplitude. The profile function $t(\mathbf{b})$ for the NN scattering can be taken as delta function if the nucleons are point particles. In general, it is taken as a Gaussian function of width r_0 as

$$t(\mathbf{b}) = \frac{\exp(-b^2/2r_0^2)}{(2\pi r_0^2)}. \quad (5)$$

Thus,

$$f_{NN}(q) = \exp(-r_0^2 q^2/2). \quad (6)$$

Here, r_0 is the range parameter and has a weak dependence on energy (see for discussions [10]). For the present work, we use $r_0 = 0.6$ fm, which is guided by the previous studies in the same energy region from Refs. [13, 7].

75 In the presence of Coulomb field, the non eikonal trajectory around the Coulomb distance of closest approach r_c is represented by $r^2 = r_c^2 + (C + 1)z^2$ [8] where r_c and the factor C are given by

$$r_c = (\eta + \sqrt{\eta^2 + b^2 k^2})/k, \quad (7)$$

$$C = \frac{\eta}{kb^2} r_c. \quad (8)$$

Here, $\eta = Z_P Z_T e^2/\hbar v$ is the dimensionless Sommerfeld parameter. In the
80 Coulomb Modified Glauber Model (CMGM) the Eq. 3 is modified as

$$\chi(b) = \frac{1}{2} \bar{\sigma}_{NN} (\bar{\alpha}_{NN} + i) AB T(r_c)/\sqrt{C + 1}. \quad (9)$$

3. Elastic Scattering Cross Section

The nucleus-nucleus differential elastic cross section as a function of center of mass angle θ is given by

$$\frac{d\sigma_{el}}{d\Omega} = |f(\theta)|^2, \quad (10)$$

where $f(\theta)$ is the sum of Coulomb and nuclear scattering amplitudes.

$$f(\theta) = f_C(\theta) + f_N(\theta). \quad (11)$$

85 For identical systems, the LHS of Eq. 10 is replaced by $|f(\theta) + f(\pi - \theta)|^2$. The Coulomb scattering amplitude is given by

$$f_C(\theta) = A_C e^{i\phi_C}, \quad (12)$$

where $A_C = -\frac{\eta}{2k} \operatorname{cosec}^2 \frac{\theta}{2}$, $\phi_C = 2\sigma_0 - 2\eta \ln \left(\sin \frac{\theta}{2} \right)$ and the nuclear scattering amplitude is

$$f_N(\theta) = \frac{1}{2ik} \sum_{l=0}^{\infty} (2l+1) (e^{2i\sigma_l}) (S_l - 1) P_l(\cos \theta). \quad (13)$$

Here, $\sigma_{l+1}(\eta) = \sigma_l(\eta) + \tan^{-1}(\frac{\eta}{l+1})$ and σ_0 can be assumed to be 0. The nuclear
90 scattering amplitude can be written as $S_l = \exp[i(\chi_R + i\chi_I)]$ and thus $f_N(\theta)$ is simplified to

$$f_N(\theta) = \frac{1}{2k} \sum_{l=0}^{\infty} (2l+1) P_l(\cos \theta) (e^{2i\sigma_l}) [N_R + iN_I], \quad (14)$$

where $N_R = [e^{-\chi_I} \sin \chi_R]$ and $N_I = [1 - e^{-\chi_I} \cos \chi_R]$.

4. The Nuclear Densities

The nuclear densities of the two nuclei are the most important inputs in the
95 model. We can calculate the Fourier transform for any given density form $\rho(r)$ to be used in Eq. (4) as follows

$$S(q) = 4\pi \int j_0(qr) \rho(r) r^2 dr \quad (15)$$

Here, $j_0(qr)$ is the spherical Bessel function of order zero. The nuclear densities are obtained by fitting electron nucleus scattering form factors measured in a momentum transfer range [30, 31]. For light nuclei such as ${}^6\text{Li}$, ${}^{12}\text{C}$ and ${}^{16}\text{O}$,
100 we use the Modified Harmonic Oscillator (MHO) density with correction for

Table 1: Density parameters of nuclei used in the present work. The parameters α and a correspond to MHO density, the parameters d and c correspond to 2pF/3pF densities and w corresponds to 3pF density. q -range is measured momentum transfer range.

Element	Form	d/α (fm)	R_{rms} (fm)	c/a (fm)	w	q -range	Ref.
$^{12}_6\text{C}$	MHO	1.247(18)	2.460	1.649(8)		1.05-4.01	[30]
$^{16}_8\text{O}$	HO	1.517	2.674	1.805(15)		0.58-0.99	[30]
$^{28}_{14}\text{Si}$	2pF	0.542(16)	3.138	3.106(30)		0.41-2.02	[30]
$^{40}_{20}\text{Ca}$	3pF	0.584	3.486	3.669	-0.102	0.49-3.37	[30]
$^{90}_{40}\text{Zr}$	2pF	0.55	4.274	4.712		-	[13]
$^{208}_{82}\text{Pb}$	2pF	0.549(8)	5.521	6.624(35)		0.22-0.88	[30]

center of mass motion [13]. For heavier nuclei such as ^{28}Si , ^{90}Zr and ^{208}Pb we use two parameter Fermi (2pF) density. We also use the three parameter Fermi (3pF) density for nuclei such as ^{40}Ca for which 2pF density is not given for wide q -range of measured form factor. The mean radius, c for ^{90}Zr has been
105 calculated using the formula given in Ref. [13].

The MHO density form is given by

$$\rho(r) = \rho_0 \left(1 + \alpha \frac{r^2}{a^2} \right) \exp \left(- \frac{r^2}{a^2} \right), \quad \rho_0 = \frac{1 + 1.5\alpha}{(\sqrt{\pi} a)^3}. \quad (16)$$

The 2pF density is given by

$$\rho(r) = \frac{\rho_0}{1 + \exp(\frac{r-c}{d})}, \quad \rho_0 = \frac{3}{4\pi c^3 [1 + \frac{\pi^2 d^2}{c^2}]} \quad (17)$$

and the 3pF density is given by

$$\rho(r) = \frac{\rho_0 (1 + \frac{wr^2}{c^2})}{1 + \exp(\frac{r-c}{d})}. \quad (18)$$

The parameters for different nuclei used in the present work are given in Table 1.

110 5. NN scattering parameters

The average NN scattering parameter $\bar{\sigma}_{NN}$ is obtained in terms of pp cross section σ_{pp} and np cross section σ_{np} averaged over proton numbers (Z_P, Z_T) and neutron numbers (N_P, N_T) of projectile and target respectively as

$$\bar{\sigma}_{NN} = \frac{N_P N_T \sigma_{nn} + Z_P Z_T \sigma_{pp} + (Z_P N_T + N_P Z_T) \sigma_{np}}{A_P A_T}. \quad (19)$$

The parametrized forms of σ_{pp} and σ_{np} are available in literature [7, 29]. The cross section σ_{pp} is assumed to be the same as σ_{pp} . We obtain new parametrization using the data from Particle Data Group [33] which are given in terms of proton lab kinetic energy E as follows

$$\sigma_{pp} = \begin{cases} -5.32 + \frac{3017.0}{E} & : 9 \leq E(\text{MeV}) \leq 90 \\ 31.74 - 0.0628 E + 1.22 \times 10^{-4} E^2 & : 90 \leq E(\text{MeV}) \leq 700 \end{cases}, \quad (20)$$

$$\sigma_{np} = \begin{cases} -1128.0 - \frac{863.0}{E} + 61.5\sqrt{E} + \frac{6170.0}{\sqrt{E}} & : 0.45 \leq E(\text{MeV}) \leq 70 \\ -8.54 + \frac{9956.0}{E} + 1.64\sqrt{E} - \frac{321.0}{\sqrt{E}} & : 70 \leq E(\text{MeV}) \leq 700 \end{cases} \quad (21)$$

The errors on the parameters in Eqs. (20) and (21) are 1-3 %. Figure 1 shows the NN cross section data [33] as a function of lab kinetic energy fitted with the functions given by Eqs. (20) and (21) along with the fits given in references [7, 29]. The data/fit graphs are shown for the present parametrizations. The Charagi-Gupta parametrization for σ_{pp} is good upto 50 MeV and that for σ_{np} is good above 10 MeV. The Bertulani-Conti parametrization of σ_{pp} differs with our parametrizations in the proton energy range 120-300 MeV and their parametrization of σ_{np} cannot be extrapolated below 8 MeV.

The average $\bar{\alpha}_{NN}$ is also calculated using α_{pp} , α_{nn} and α_{np} as follows

$$\bar{\alpha}_{NN} = \frac{N_P N_T \alpha_{nn} \sigma_{nn} + Z_P Z_T \alpha_{pp} \sigma_{pp} + (Z_P N_T + N_P Z_T) \alpha_{np} \sigma_{np}}{\sigma_{NN} A_P A_T}. \quad (22)$$

The parametrizations for quantities α_{pp} and α_{np} as a function of lab kinetic energy are obtained using the data of phase shift analysis given in Ref. [34]

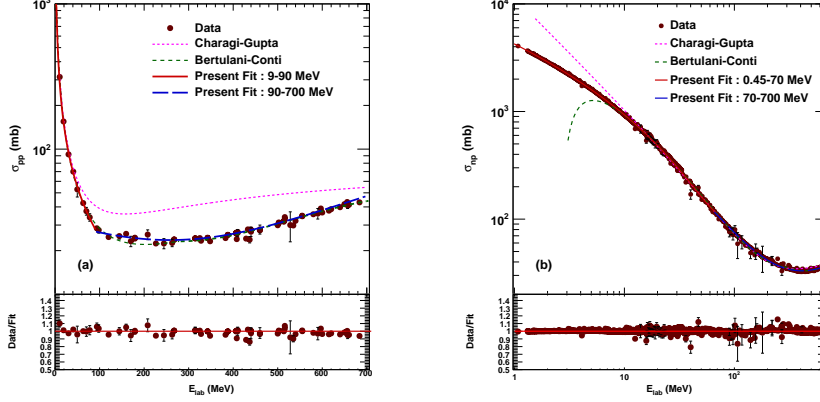


Figure 1: (a) proton-proton cross section and (b) neutron-proton cross section data as a function of lab kinetic energy [33] fitted with the functions given by Eqs. (20) and (21) along with the fits which are given in references [7, 29].

which is in accordance with the experimental data. It is assumed that $\alpha_{nn} =$
 130 α_{pp} . The present parametrizations are obtained for proton lab energy E between
 7 to 260 MeV given as

$$\alpha_{pp} = a_p + b_p E + c_p E^2 + d_p E^3 \quad E \text{ (in MeV)}, \quad (23)$$

where $a_p = 0.435$, $b_p = 3.202 \times 10^{-2}$, $c_p = -2.287 \times 10^{-4}$ and $d_p = 4.134 \times 10^{-7}$
 and

$$\alpha_{np} = a_n + b_n E + c_n E^2 + d_n E^3 \quad E \text{ (in MeV)}, \quad (24)$$

where $a_n = -0.3695$, $b_n = 3.211 \times 10^{-2}$, $c_n = -2.117 \times 10^{-4}$ and $d_n = 3.672 \times$
 135 10^{-7} . The errors on these parameters are 7-10 %.

Figure 2 shows the ratio of real to imaginary part of NN scattering amplitude
 as a function of lab kinetic energy from phase shift analysis of Ref. [34] fitted
 with the functions given by Eqs. (23) and (24) along with the fit which was
 given in Ref. [7]. The earlier parametrization [7] for α_{pp} and α_{np} were good
 140 below 60 MeV.

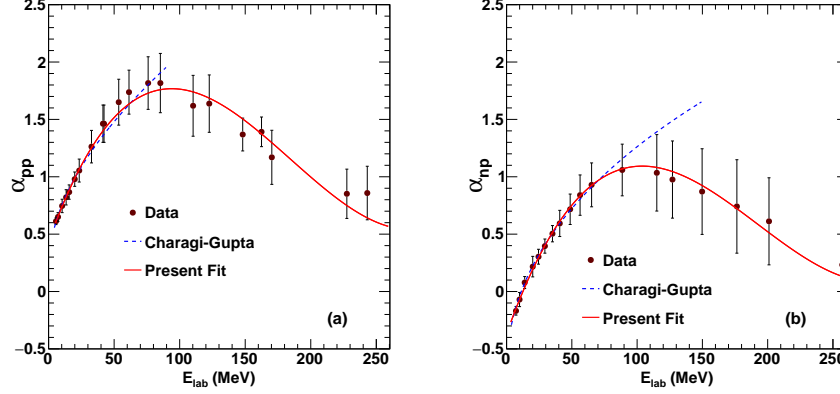


Figure 2: The ratio of real to imaginary part of NN scattering amplitude (a) α_{pp} and (b) α_{np} as a function of lab kinetic energy obtained from phase shift analysis of Ref. [34] fitted with the functions given by Eqs. (23) and (24) along with the fit which was given in Ref. [7].

6. Results and discussions

We calculate σ_R as a function of lab kinetic energy per nucleon E/A and $\frac{d\sigma_{el}}{d\sigma_{Ruth}}$ as a function of θ_{cm} for various reaction combinations of light, medium and heavy nuclei and compare with the data. The reaction cross section data
145 are obtained by optical model analysis of measured elastic scattering angular distributions. Such analysis is mostly provided by the experimental group. In case the error on the cross section is not given a 5 % error is assumed which is typically the error obtained in such analysis. The errors on the input parameters, NN cross sections and density parameters are propagated in the final
150 calculations. The uncertainty bands also include an 8 % variation in the nuclear range parameter r_0 around 0.6 fm.

Figure 3 shows the total reaction cross section as a function of lab kinetic energy per nucleon for $^{12}\text{C} + ^{12}\text{C}$ system [35, 36, 37]. For this system we have put 5 % error on the cross section data at $E/A = 8.567, 30$ and 120.75 MeV.
155 Figure 4 (a) shows the total reaction cross section as a function of lab kinetic energy per nucleon for $^{16}\text{O} + ^{16}\text{O}$ system [38, 39, 40] and the Fig. 4 (b) shows the same for $^{16}\text{O} + ^{12}\text{C}$ system [41, 42, 43, 44, 45, 46]. The band is CMGM

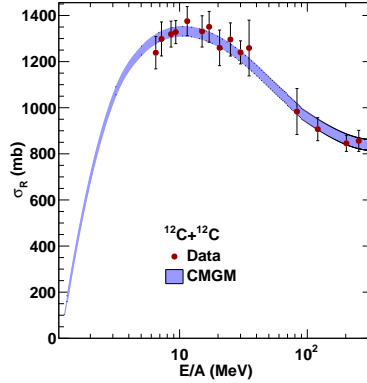


Figure 3: The total reaction cross section as a function of lab kinetic energy per nucleon for $^{12}\text{C} + ^{12}\text{C}$ system [35, 36, 37].

which includes the uncertainties on the input parameters. The model gives very good description of the data for all the light systems except at very low energies far below Coulomb barrier for $^{16}\text{O} + ^{16}\text{O}$ system.

Figure 5 (a) shows the total reaction cross section as a function of lab kinetic energy per nucleon for $^{12}\text{C} + ^{28}\text{Si}$ system [42] and the Fig. 5 (b) shows the same for $^{16}\text{O} + ^{28}\text{Si}$ system [47]. For all the data shown in figures 4 and 5 we have put 5 % error on the reaction cross section. Figure 6 (a) shows the total reaction cross section as a function of lab kinetic energy per nucleon for $^{12}\text{C} + ^{40}\text{Ca}$ system [35, 44] and the Fig. 6 (b) shows the same for $^{12}\text{C} + ^{90}\text{Zr}$ system [35, 44, 48]. The band is CMGM which includes the uncertainties on the input parameters. The model gives good description of the data for medium mass systems except for the $^{12}\text{C} + ^{90}\text{Zr}$ system. For $^{12}\text{C} + ^{40}\text{Ca}$ system at energy $E/A = 3.75$ MeV we have put a 5 % error on the reaction cross section. Similar error was put in the cross section for the system $^{12}\text{C} + ^{90}\text{Zr}$ at energies $E/A = 8.166$ and 35 MeV.

Figure 7 (a) shows the total reaction cross section as a function of lab kinetic energy per nucleon for $^{12}\text{C} + ^{208}\text{Pb}$ system [35, 48, 49]. Figure 7 (b) shows the same for $^{16}\text{O} + ^{208}\text{Pb}$ system [50, 51, 52, 53, 54, 55]. The band is CMGM which

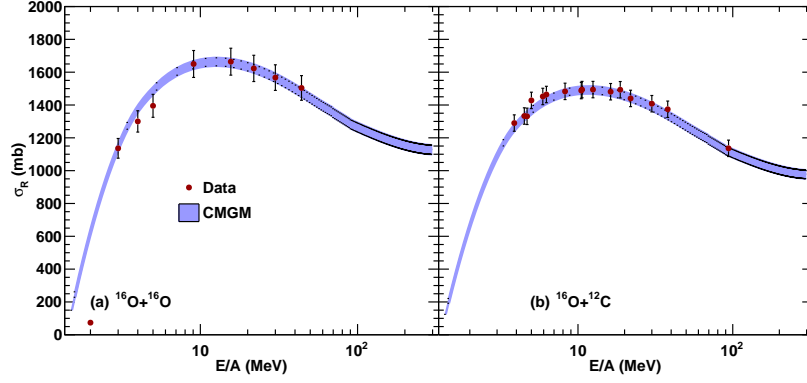


Figure 4: The total reaction cross section as a function of lab kinetic energy per nucleon for (a) $^{16}\text{O} + ^{16}\text{O}$ system [38, 39, 40] and (b) $^{16}\text{O} + ^{12}\text{C}$ system [41, 42, 43, 44, 45, 46].

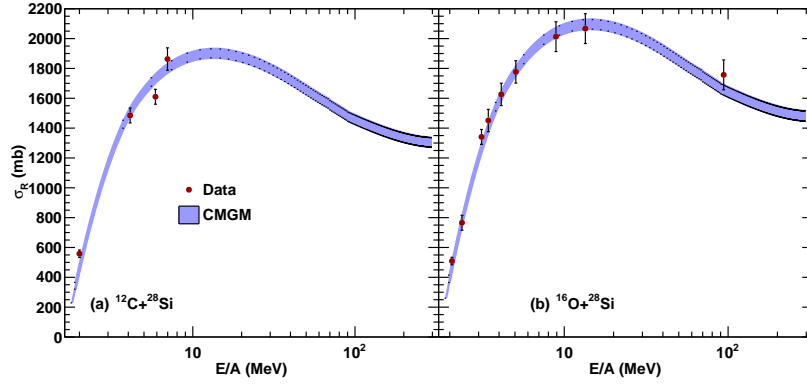


Figure 5: The total reaction cross section as a function of lab kinetic energy per nucleon for (a) $^{12}\text{C} + ^{28}\text{Si}$ system [42] and (b) $^{16}\text{O} + ^{28}\text{Si}$ system [47].

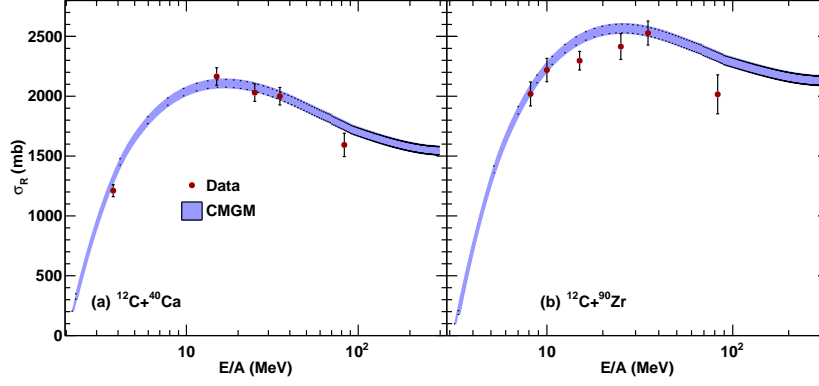


Figure 6: The total reaction cross section as a function of lab kinetic energy per nucleon for (a) $^{12}\text{C} + ^{40}\text{Ca}$ system [35, 44] and (b) $^{12}\text{C} + ^{90}\text{Zr}$ system [35, 44, 48].

includes the uncertainties on the input parameters. For $^{12}\text{C} + ^{208}\text{Pb}$ system at energies $E/A = 8$ and 9.66 MeV we have put a 5 % error on the reaction cross section. Similar error was put in the cross section for the system $^{16}\text{O} + ^{208}\text{Pb}$ at energies $E/A = 6.0, 8.093, 12.0$ and 19.54 MeV.

180 The model gives very good description of the data for both the heavy systems considered here. We can conclude that the reaction cross section calculations from the model are very reliable and thus the model can be used to predict the reaction cross section for unknown systems. It can also be used to obtain radii of nuclei from measured reaction cross section.

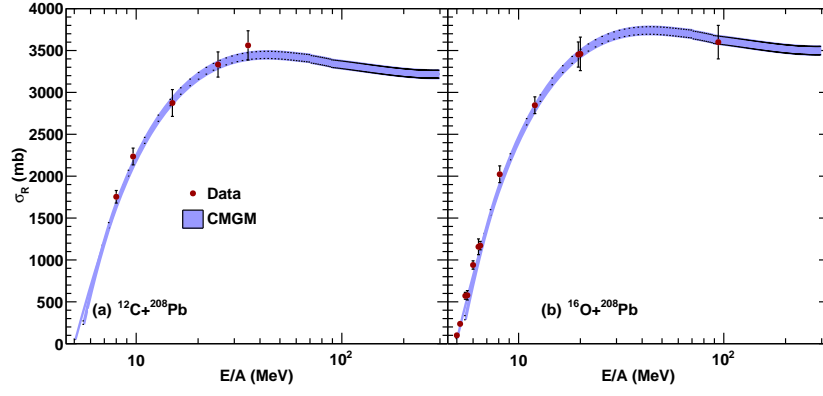


Figure 7: The total reaction cross section as a function of lab kinetic energy per nucleon for (a) $^{12}\text{C} + ^{208}\text{Pb}$ system [35, 48, 49] and (b) $^{16}\text{O} + ^{208}\text{Pb}$ system [50, 51, 52, 53, 54, 55, 46].

185 Figures 8 shows the measured ratio of elastic scattering cross section to the
Rutherford cross section as a function of scattering angle for $^{12}\text{C} + ^{12}\text{C}$ system
at three energies given in (a) $E/A = 15$ MeV [56], (b) $E/A = 30$ MeV [49, 57, 58]
and (c) $E/A = 84.66$ MeV [49, 57] along with the CMGM calculations shown
by bands. Figure 9 shows the measured ratio of elastic scattering cross section
190 to the Rutherford cross section as a function of scattering angle for $^{16}\text{O} + ^{16}\text{O}$
system for three energies given in (a) $E/A = 8.12$ MeV [59] (b) $E/A = 44$ MeV
[60, 61] and (c) $E/A = 70$ MeV [60] along with the CMGM calculations shown
by bands.

The parameter $\bar{\alpha}_{NN}$ is obtained by fitting the experimental data on angular
195 distribution which is given in the Table 2 along with the values obtained using
parametrizations given by Eqs. (23) and (24). The model produces the measured
diffractive oscillations but the oscillation magnitudes in the data in the light
systems are more pronounced as compared to the oscillations observed in the
data specially at higher energies and higher angles i.e. at the higher momentum
200 transfer. The parameter $\bar{\alpha}_{NN}$ does not control oscillation magnitude, but affects
the slope (inclination) of $d\sigma/d\sigma_{Ruth}$ as a function of θ_{cm} .

Figure 10 shows the measured ratio of elastic scattering cross section to the
Rutherford cross section as a function of scattering angle for $^{12}\text{C} + ^{40}\text{Ca}$ system
[35] for two energies given in (a) $E/A = 25$ MeV and (b) $E/A = 35$ MeV along
205 with the CMGM calculations shown by bands.

Figure 11 shows the measured ratio of elastic scattering cross section to the
Rutherford cross section as a function of scattering angle for $^{12}\text{C} + ^{90}\text{Zr}$ system
[35] for two energies given in (a) $E/A = 15$ MeV and (b) $E/A = 35$ MeV along
with the CMGM calculations shown by bands.

210 Figure 12 shows the measured ratio of elastic scattering cross section to the
Rutherford cross section as a function of scattering angle for $^{12}\text{C} + ^{208}\text{Pb}$ system
[35, 62] for two energies given in (a) $E/A = 25$ MeV and (b) $E/A = 85.83$ MeV
along with the CMGM calculations shown by bands.

Figure 13 shows the measured ratio of elastic scattering cross section to the
215 Rutherford cross section as a function of scattering angle for $^{16}\text{O} + ^{208}\text{Pb}$ system

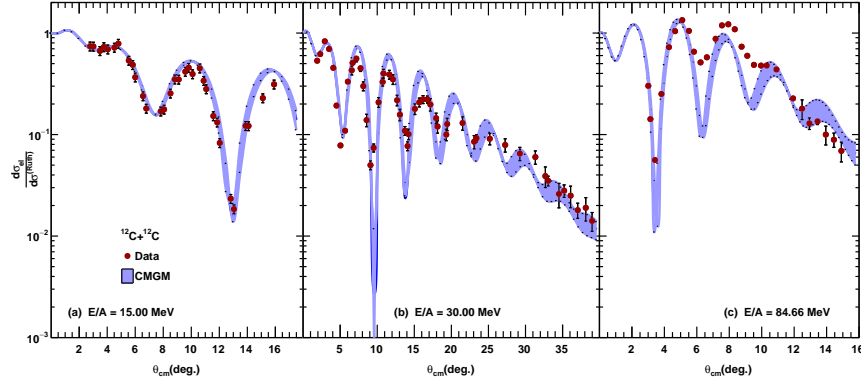


Figure 8: The measured ratio of elastic scattering cross section to the Rutherford cross section as a function of scattering angle for $^{12}\text{C} + ^{12}\text{C}$ system at (a) $E/A = 15$ MeV [56], (b) $E/A = 30$ MeV [49, 57, 58] and (c) $E/A = 84.66$ MeV [49, 57] along with the CMGM calculations.

[53, 46] for two energies given in (a) $E/A = 12$ MeV and (b) $E/A = 93.75$ MeV along with the CMGM calculations shown by bands.

The fitted values of the parameter $\bar{\alpha}_{NN}$ for all the systems are given in the Table 2. For heavy ion systems this parameter does not follow the same energy
 220 dependence shown by NN scattering and approaches towards one for all the systems. The model produces the measured elastic scattering angular distributions for medium and heavy systems at low energies but, at higher energies the model produces diffractive oscillations of larger magnitude as compared to the data.

The large oscillations in the model at high momentum transfer may be the
 225 consequence of assuming a semiclassical picture of scattering in terms of impact parameter and distance of closest approach. The Glauber optical potential in terms of densities of the two nuclei and NN amplitude does not always reproduce the features of data at large scattering angles. An improved fitting should be obtained by having more free parameters in the nuclear potential/interactions
 230 shown in the studies in Ref. [23] or in Ref. [27].

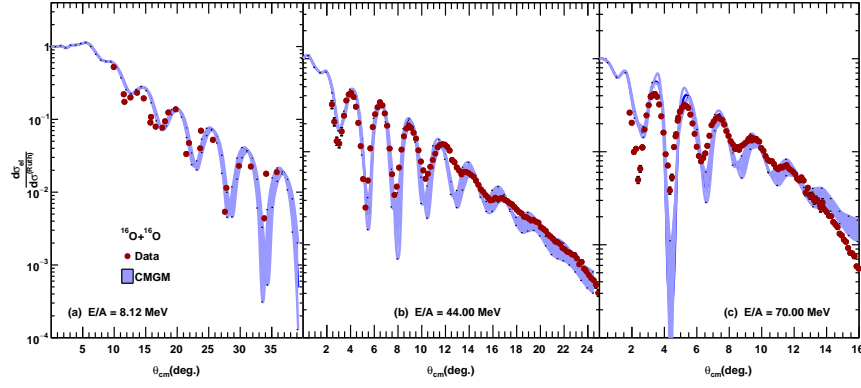


Figure 9: The measured ratio of elastic scattering cross section to the Rutherford cross section as a function of scattering angle for $^{16}\text{O} + ^{16}\text{O}$ system at (a) $E/A = 8.12$ MeV [59] (b) $E/A = 44$ MeV [60, 61] and (c) $E/A = 70$ MeV [60] along with the CMGM calculations.

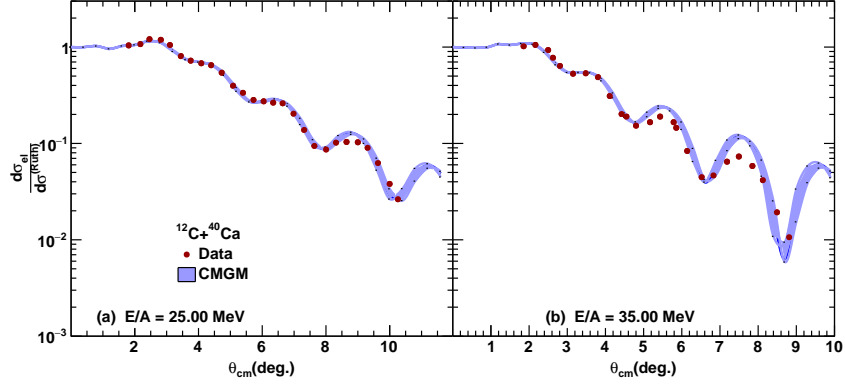


Figure 10: The measured ratio of elastic scattering cross section to the Rutherford cross section as a function of scattering angle for $^{12}\text{C} + ^{40}\text{Ca}$ system [35] at (a) $E/A = 25$ MeV and (b) $E/A = 35$ MeV along with the CMGM calculations shown by bands.

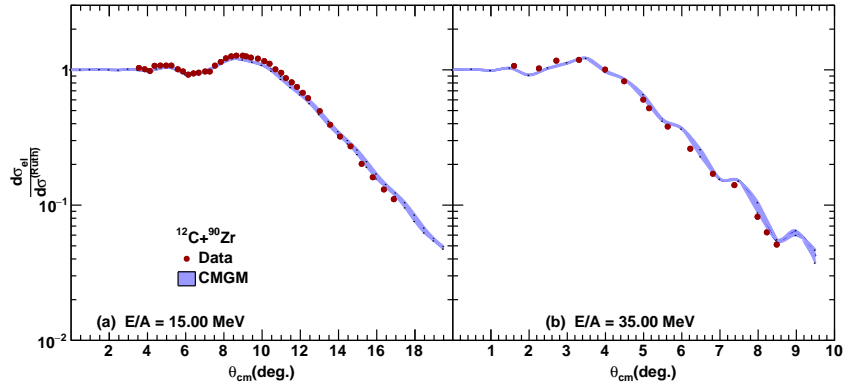


Figure 11: The measured ratio of elastic scattering cross section to the Rutherford cross section as a function of scattering angle for $^{12}\text{C} + ^{90}\text{Zr}$ system [35] at (a) $E/A = 15$ MeV and (b) $E/A = 35$ MeV along with the CMGM calculations shown by bands.

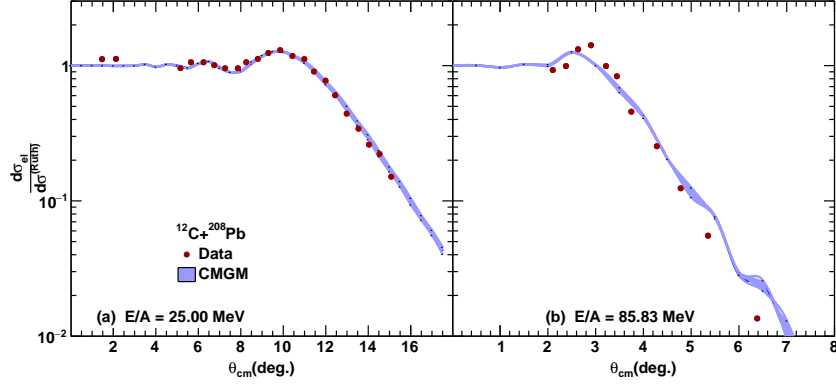


Figure 12: The measured ratio of elastic scattering cross section to the Rutherford cross section as a function of scattering angle for $^{12}\text{C} + ^{208}\text{Pb}$ system [35, 62] at (a) $E/A = 25$ MeV and (b) $E/A = 85.83$ MeV along with the CMGM calculations shown by bands.

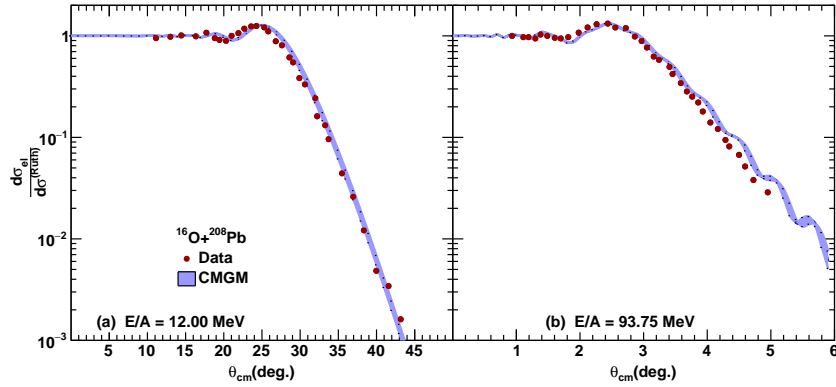


Figure 13: The measured ratio of elastic scattering cross section to the Rutherford cross section as a function of scattering angle for $^{16}\text{O} + ^{208}\text{Pb}$ system [53, 46] at (a) $E/A = 12$ MeV and (b) $E/A = 93.75$ MeV along with the CMGM calculations shown by bands.

Table 2: Calculated (from parametrization) and fitted values of $\bar{\alpha}_{NN}$.

System	E/A (MeV)	$\bar{\alpha}_{NN(\text{calc})}$	$\bar{\alpha}_{NN(\text{fitted})}$
$^{12}\text{C} + ^{12}\text{C}$	15.00	0.255	0.9
	30.00	0.595	0.78
	84.66	1.25	0.9
$^{16}\text{O} + ^{16}\text{O}$	8.12	0.1	0.80
	44.00	0.85	0.94
	70.00	1.165	1.02
$^{12}\text{C} + ^{40}\text{Ca}$	25.00	0.488	0.8
	35.00	0.694	1.0
$^{12}\text{C} + ^{90}\text{Zr}$	15.00	0.255	0.7
	35.00	0.694	1.0
$^{12}\text{C} + ^{208}\text{Pb}$	25.00	0.48	1.0
	85.83	1.25	1.254
$^{16}\text{O} + ^{208}\text{Pb}$	12.00	0.181	1.0
	93.75	1.272	1.5

7. Conclusions

We calculate the heavy ion reaction cross sections and elastic scattering angular distributions at low and intermediate energies using Glauber model and test the calculations with the available measured data. We present new parametrization for the data of total cross sections as well as for the ratio of real to imaginary parts of the scattering amplitudes in case of pp and np collisions. The model works at low energies down to Coulomb barrier with very simple modifications. The reaction cross section calculations from the model are very reliable and thus the model can be used to predict the reaction cross section for unknown systems. It can also be used to obtain radii of nuclei from measured reaction cross sections in low and intermediate energy range.

The model describes the measured elastic scattering angular distributions having diffractive oscillations but the oscillation magnitude in the data is more

pronounced as compared to the oscillations observed in the data specially at
 245 higher energies and higher angles i.e. at the higher momentum transfer. For
 heavy ion systems, the parameter $\bar{\alpha}_{NN}$ does not follow the same energy dependence
 shown by NN scattering and approaches towards one for all the systems.

References

References

- 250 [1] R. J. Glauber, *Lectures on theoretical Physics*, Vol. I, Inter-Science, New
 York (1959).
- [2] P. J. Karol, Phys. Rev. **C11** (1975) 1203.
- [3] C.Y. Wong, *Introduction to High Energy Heavy Ion Collisions*, World Sci-
 entific, Singapore (1994).
- 255 [4] P. Shukla, Preprint: nucl-th/0112039 (2001).
- [5] D. G. d'Enterria, nucl-ex/0302016.
- [6] A. Vitturi and F. Zardi, Phys. Rev. **C36** (1987) 1404; S.M. Lenzi, A. Vit-
 turi, F. Zardi, Phys. Rev. **C40** (1989) 2114.
- [7] S. K. Charagi and S. K. Gupta, Phys. Rev. **C41** (1990) 1610; Phys. Rev.
 260 **C46** (1992) 1982.
- [8] S. K. Gupta and P. Shukla, Phys. Rev. **C52** (1995) 3212.
- [9] R. E. Warner, M. H. McKinnon, and H. Thirumurthy and A. Nadasen,
 Phys. Rev. **C59** (1999) 1215.
- [10] I. Ahmad, M. A. Abdulmomen, and M. S. Al-Enazi, Phys. Rev. **C65** (2002)
 265 054607.
- [11] X. Z. Cai, J. Feng, W. Q. Shen, Y. G. Ma, J. S. Wang and W. Ye, Phys.
 Rev. C **58** (1998) 572.

- [12] A. de Vismes, P. Roussel-Chomaz, and F. Carstoiu, Phys. Rev. C **62** (2000) 064612.
- 270 [13] P. Shukla, Phys. Rev. C **67** (2003) 054607.
- [14] G. D. Alkhazovi, Y. Shabelski and I. S. Novikov, Int. J. Mod. Phys. E **20** (2011) 583 [arXiv:1101.4717 [nucl-th]].
- [15] I. Tanihata et al., Phys. Rev. Lett. **55** (1985) 2676; I. Tanihata, Nucl. Phys. A **488** (1988) 113c; I. Tanihata et. al, Phys. Lett. B **289** (1992) 261.
- 275 [16] W. Horiuchi, Y. Suzuki, B. Abu-Ibrahim and A. Kohama, Phys. Rev. C **75** (2007) 044607. Erratum: [Phys. Rev. C **76** (2007) 039903]. [nucl-th/0612029].
- [17] S. K. Patra, R. N. Panda, P. Arumugam and R. K. Gupta, Phys. Rev. C **80** (2009) 064602.
- 280 [18] M. K. Sharma and S. K. Patra, Phys. Rev. C **87** (2013) 044606.
- [19] D. Chauhan, Z. A. Khan and A. A. Usmani, Phys. Rev. C **90** (2014) 024603.
- [20] M. Y. M. Hassan, M. Y. H. Farag, A. Y. Abul-Magd and T. E. I. Nassar, Phys. Scripta **78** (2008) 045202 [arXiv:0902.0453 [nucl-th]].
- [21] J. A. Christley and J. A. Tostevin, Phys. Rev. C **59** (1999) 2309.
- 285 [22] V. K. Lukyanov, D. N. Kadrev, E. V. Zemlyanaya, K. Spasova, K. V. Lukyanov, A. N. Antonov and M. K. Gaidarov, Phys. Rev. C **91** (2015) 034606. [arXiv: 1502.06425 [nucl-th]].
- [23] Dao T. Khoa, W. von Oertzen, H. G. Bohlens and F. Nuoffer, Nucl. Phys. A **672** (2000) 387.
- 290 [24] M. M. H. El-Gogary, A. S. Shalaby, M. Y. M. Hassan and A. M. Hegazy, Phys. Rev. C **61** (2000) 044604.
- [25] M. M. H. El-Gogary, A. S. Shalaby and M. Y. M. Hassan, Phys. Rev. C **58** (1998) 3513.

- [26] F. Sammarruca and L. White, Phys. Rev. C **83** (2011) 064602. [arXiv: 1105.5666 [nucl-th]].
- [27] I. AHMAD and M. A. ALVI, Int. J. Mod. Phys. E **13** (2000) 1225.
- [28] W. R. Gibbs and J. P. Dedonder, Phys. Rev. C **86** (2012) 024604. [arXiv: 1203.0019 [nucl-th]].
- [29] C. A. Bertulani and C. De Conti, Phys. Rev. C **81** (2010) 064603. [arXiv:1004.2096 [nucl-th]].
- [30] C. W. de Jager, H. de Vries and C. de Vries, Atom. Nucl. Data Tables **14** (1974) 479.
- [31] H. De Vries, C. W. de Jager, and C. de Vries, Atom. Nucl. Data Tables **36** (1987) 495.
- [32] V. Franco and A. Tekou, Phys. Rev. C **16** (1987) 658.
- [33] Particle Data Group, (<http://pdg.lbl.gov/2014/hadronic-xsections/>).
- [34] W. Grein, Nucl. Phys. B **131** (1977) 255.
- [35] C. C. Sahm et. al, Phys. Rev. C **34** (1986) 2165.
- [36] M. A. Hassanain, A. A. Ibraheem and M. E. Farid, Phys. Rev. C **77** (2008) 034601.
- [37] J. Y. Histachy et. al, Nucl. Phys. A **490** (1998) 441.
- [38] R. Bass, *Nuclear reactions with heavy ions*, (Springer-Verlag, NY), 1980.
- [39] Dao T. Khoa, W. von Oertzen, H. G. Bohlen, G. Bartnitzky, H. Clement, Y. Sugiyama, B. Gebauer, A. N. Ostrowski, Th. Wilpert, M. Wilpert, and C. Langner, Phys. Rev. Lett. **74** (1995) 34.
- [40] M. A. Hassanain, A. A. Ibraheem, S. M. M. Al Sebiey, S. R. Mokhtar, M. A. Zaki, Z. M. M. Mahmoud, K. O. Behairy and M. E. Farid, Phys. Rev. C **87** (2013) 064606.

- [41] M. P. Nicoli, F. Haas, R. M. Freeman, S. Szilner, Z. Basrak, A. Morsad,
320 G. R. Satchler and M. E. Brandan, Phys. Rev. **C61** (2000) 034609.
- [42] M. El-Azab Farid, Z. M. M. Mahmoud and G.S. Hassan, Nucl. Phys. **A691**
(2001) 671.
- [43] A. A. Ogloblin et. al, Phys. Rev. **C62** (2000) 044601.
- [44] G. R. Satchler and W.G. Love, Phys. Rep. **55** (1979) 183.
- [45] M. E. Brandan et. al, Nucl. Phys. **A688** (2001) 659.
325
- [46] P. Roussel-Chomaz et. al, Nucl. Phys. **A477** (1988) 345.
- [47] J.G. Cramer, R.M. Devries, D.A. Goldberg, M.A. Zisman and C.F.
Maguire, Phys. Rev. **C14** (1976) 2158.
- [48] M. E. Brandan, H. Chehime and K. W. McVoy, Phys. Rev. **C55** (1997)
330 1353.
- [49] M. Buenerd et. al, Phys. Lett. **B102** (1981) 242.
- [50] Louis C. Vaz, John M. Alexander, E. H. Auerbach, Phys. Rev. **C18** (1978)
820.
- [51] F. D. Becheti, Phys. Rev. **C6** (1972) 2215.
- [52] J. B. Ball, C. B. Fulmer, E. E. Gross, M. L. Halbert, D. C. Hensley, C. A.
335 Ludemann, M. J. Saltmarsh and G. R. Satchler, Nucl. Phys. **A252** (1975)
208.
- [53] S. K. Charagi, Phys. Rev. **C51** (1995) 3521.
- [54] C. Olmer et.al, Phys. Rev.**18** (1978) 205.
- [55] K. W. McVoy and W. A. Friedman, *Theoretical Methods in Medium-Energy
340 and Heavy-Ion Physics*, Springer US (1978).
- [56] Dao T. Khoa, W. von Oertzen, and H. G. Bohlen, Phys. Rev. **C 49** (1994)
1652.

- [57] M. Buenerd et. al, Phys. Rev. C**26** (1982) 1299.
- 345 [58] M. C. Mermaz, Nucl. Phys. A**424** (1984) 313.
- [59] H. Ikezoe et. al, Nucl. Phys. A**456** (1986) 298.
- [60] F. Nuoffer et. al, Nuovo Cimento A**111** (1998) 971.
- [61] G. Bartnitzky et. al, Phys. Lett. B**365** (1996) 23.
- [62] M. A. G. Alvarez, L. C. Chamon, M. S. Hussein, D. Pereira, L. R. Gasques,
 350 E. S. Rossi, Jr. and C. P. Silva, Nucl. Phys. A **723** (2003) 93. [nucl-
 th/0210062].